Model Predictive Current Control of Mutually Coupled Switched Reluctance Machines using a Three-Phase Voltage Source Converter

Kun Hu, Lulu Guo and Jin Ye
Intelligent Power Electronics and Electric Machine Laboratory
School of Electrical and Computer Engineering
University of Georgia, Athens, Georgia 30602
Email: kun.hu@uga.edu, lulu.guo@uga.edu, jin.ye@uga.edu

Abstract—In this paper, a model predictive current controller (MPCC) is proposed for short-pitched mutually coupled switched reluctance machines (MCSRMs) using a three-phase voltage source converter (VSC) to achieve fast dynamics and advanced current tracking ability. Due to strong mutually coupling between phases, to our knowledge, MPCC for MCSRMs has not been studied yet. A two-order flux-based prediction model of the MCSRMs using the VSC is presented with standard state space equations in discrete-time domain, based on which, the current regulation is achieved by solving a constrained optimization problem. With the receding optimal duty ratio input, MPCC demonstrates good current tracking ability, which is verified by simulations with a three-phase, sinusoidal excitation 12/8 MCSRM. Compared to hysteresis current control, the current response with MPCC bears lower current ripples and a fixed switching frequency.

I. Introduction

Switched reluctance machines (SRMs) are currently emerging as promising solutions to electric vehicles, domestic appliances and industrial applications, primarily due to their rigidity, non-reliance on rare-earth permanent magnet materials, and extended-speed constant-power range [1]–[3]. Mutually coupled switched reluctance machines (MCSRMs) inherit important benefits of conventional switched reluctance machines (SRMs) and offer further advantages, such as lower copper and iron losses, higher fault tolerance, flexible drive schemes and less sensitivity to magnetic saturation [4]–[7].

One distinctive advantage of the MCSRMs is that they can be driven by a three-phase voltage source converter (VSC) with either bipolar square-waveform or sinusoidal-waveform current excitation [8] because at least two phases should be conducting to generate mutual inductances. The closest work of current control for MCSRM with VSC is done in [9] using sinusoidal current excitation for acoustic noise reduction for MCSRMs.

Traditionally, PWM-based control or hysteresis control methods are adopted to manipulate the converter switches in order to generate desired terminal voltages for machines. The hysteresis control method is widely employed due to its simplicity, fast dynamic response, and independence of motor models but suffers from variable switching frequency

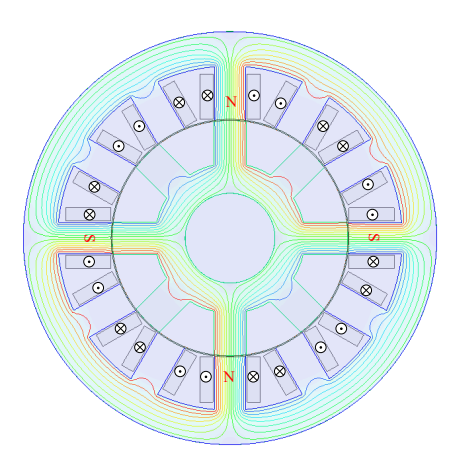


Fig. 1 Winding distribution and flux lines of the conventional SRM.

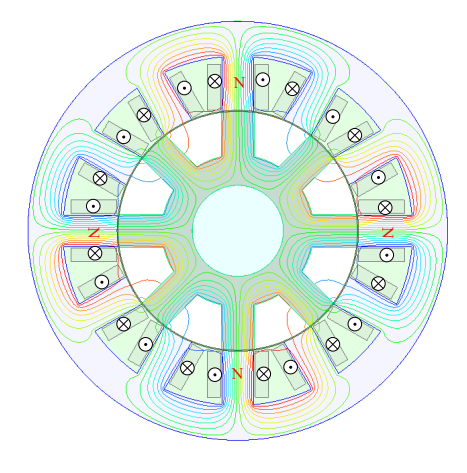


Fig. 2 Winding distribution and flux lines of the short-pitched MCSRM.

and much higher sampling rate. The fixed-switching-frequency sliding mode control method was then incorporated into both SRMs and MCSRMs [10], [11] to address the problem. If the inductance is small and back EMF is low at the lower speeds,

the machine often suffers from high current ripples [12]. Model predictive control (MPC) techniques show promise in optimizing switching frequency and current ripples simultaneously. MPC method is capable of deriving the optimal control signals for the switches in a more intuitive way, i.e., solving the cost function to minimize the tracking errors in a specified sampling period. One of the successful MPC applications for power converters is the finite control set MPC, which takes advantage of the converter's feature of having finite switching states. Thus, through the finite computation of possible future switching states, then selecting the one with the minimum cost for the next stage, the optimal problem can be solved. Details of single-step or multi-step prediction of the future switching states for power converters can be found in [13].

In addition to the application for power converters, finite control set MPC has also been explored in electric machines with predicting the optimal duty ratio for each phase. Specifically, MPC has been an attractive technique for current and torque control for SRMs with the advantage of easy inclusion of model nonlinearities and constraints [14]-[19] where the torque and current ripples and switching frequency can be minimized. However, this method suffers from a heavy computation burden and high reliance on an accurate model. To overcome the drawbacks, [17] proposed the deadbeat (singlestep) predictive current controller to predict the duty ratio for the asymmetric converter with accurate inductance profiles. Paper [14] developed a stochastic MPC with adaptive model calibration to address the model uncertainty and measurement noise issue. Compared to the conventional SRMs, MCSRMs bear more mutual coupling between phases due to the utilization of VSC, which makes it a worthwhile attempt to apply MPC for MCSRMs. However, the relevant MPC technique for MCSRMs has yet to be explored. And previous works for SRMs with asymmetric bridge converter cannot be directly applied to MCSRMs.

In this paper, a finite control set MPCC is firstly developed for a short-pitched MCSRM (Fig. 2) to gain fast dynamic and accurate current tracking. In section II, a two-order flux-based model of the MCSRM and the VSC is presented with state-space equations. Section III presents the problem formulation and derivation of the optimal solution to the constrained finite control set MPC problem. Followed by that, the effectiveness of MPCC, the selection of switching frequency and prediction horizon are discussed through simulation in section IV. Conclusions are given in section V.

II. FLUX-BASED DYNAMIC MODEL OF THE MCSRMS

In this section, a three-phase 12/8 short-pitched MCSRM has been selected as the plant. Finite Element Analysis (FEA) is conducted to depict the electromagnetic characteristics of the investigated machine. Fig. 3 shows the self inductance and mutual inductance profiles of the MCSRM under single-phase constant current excitation and three-phase sinusoidal current excitation. It can be observed that both self and mutual inductance profiles are almost overlapped under the two different excitation ways, which provides the proof that

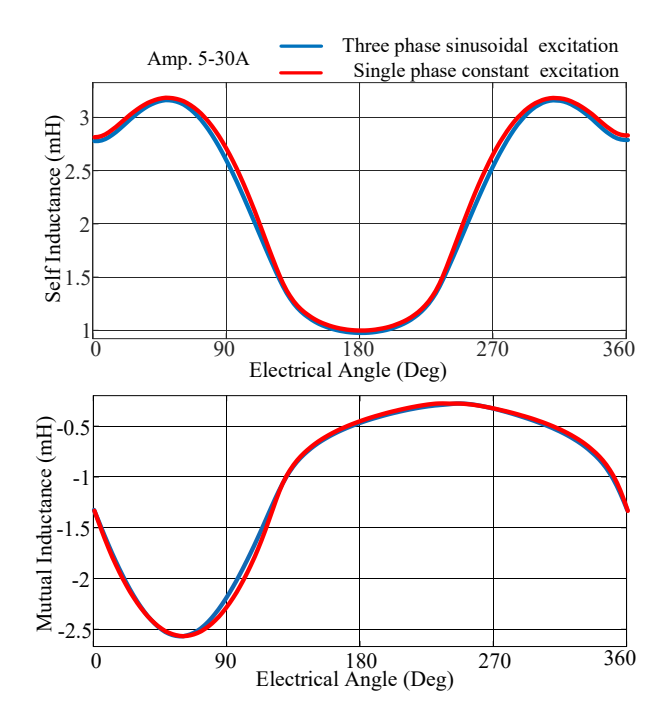


Fig. 3 Inductance profiles under two current excitations.

the investigated machine works in the linear magnetic region around the rated operating current of 15A, and thus can be modeled as a linear time variant drive system.

The previous modeling of the MCSRM for current control adopts current-based dynamic equations [10], [20]. However, the terms to describe the derivative of the inductances make it inferior to apply MPC methods compared to a flux-based model [16], which is valid for MCSRMs because there are more similar terms involved considering mutual inductance. Therefore, in this paper we use the flux-based model to form the MPC given by

$$\dot{\psi}(t) = -R_s G \psi(t) + v(t), \tag{1}$$

$$i(t) = G\psi(t), \tag{2}$$

where $\psi(t) = [\psi_A \ \psi_B \ \psi_C]^T$, $v(t) = [v_{AO} \ v_{BO} \ v_{CO}]^T$, $i(t) = [i_A \ i_B \ i_C]^T$ are the three-phase flux linkage, terminal voltages and phase currents, respectively; R_s is stator ohmic resistance for each phase;

$$G = \left[\begin{array}{c} L_A \ M_{AB} \ M_{AC} \\ M_{AB} \ L_B \ M_{BC} \\ M_{AC} \ M_{BC} \ L_C \end{array} \right]^{-1} := \left[\begin{array}{c} G_{11} \ G_{12} \ G_{13} \\ G_{21} \ G_{22} \ G_{23} \\ G_{31} \ G_{32} \ G_{33} \end{array} \right].$$

The variables included in G are defined as: L_k are self-inductance of kth phase (k=A,B,C), respectively; M_{AB},M_{AC} and M_{BC} are the mutual inductances between adjacent conducting phases. It should be noted that the inductances are associated with phase current and rotor position, e.g., $L_k = L_k(i_k,\theta_k)$. Considering that the investigated MC-SRM is less sensitive to magnetic saturation, $L_k \approx L_k(\theta_k)$.

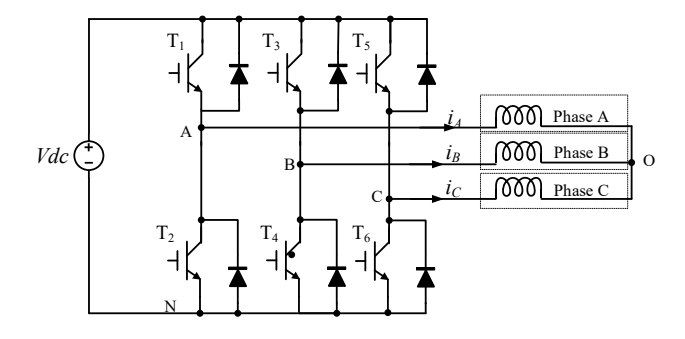


Fig. 4 Three phase MCSRM driven by standard voltage source converter.

Different from the conventional SRMs where each stator winding is individually controlled by corresponding bridge leg of the asymmetric bridge converter, the modeling of the MCSRM needs to be combined with the voltage source converter (Fig. 4) given that the three-phase terminal voltages are coupled by the converter topology. In order to derive the control input $\begin{bmatrix} v_{AN} & v_{BN} & v_{CN} \end{bmatrix}^T$ for the VSC, the averaged model of the VSC described by the three-phase duty ratio $D = \begin{bmatrix} d_A & d_B & d_C \end{bmatrix}^T$ is given by

$$\begin{bmatrix} v_{AO} \\ v_{BO} \\ v_{CO} \end{bmatrix} = \begin{bmatrix} \frac{2}{3} & -\frac{1}{3} & -\frac{1}{3} \\ -\frac{1}{3} & \frac{2}{3} & -\frac{1}{3} \\ -\frac{1}{3} & -\frac{1}{3} & \frac{2}{3} \end{bmatrix} \begin{bmatrix} v_{AN} \\ v_{BN} \\ v_{CN} \end{bmatrix}$$
$$= \begin{bmatrix} \frac{2}{3} & -\frac{1}{3} & -\frac{1}{3} \\ -\frac{1}{3} & \frac{2}{3} & -\frac{1}{3} \\ -\frac{1}{3} & -\frac{1}{3} & \frac{2}{3} \end{bmatrix} \begin{bmatrix} d_A \\ d_B \\ d_C \end{bmatrix} V_{dc}. \tag{3}$$

For now, the flux-based state-space model of the three-phase drive system has been established by substituting the voltage vector in (1) with (3). However, the modeling is not accurate because a critical feature of the drive system is not included, that is, $i_A+i_B+i_C=0$. In other words, the three-phase flux linkage associated with three-phase currents are not independent of each other. Instead, one state variable can be expressed by the combination of the rest two state variables. In this case, the following equation can be derived:

$$\psi_C(t) = H \left[\psi_A(t) \ \psi_B(t) \right]^T, \tag{4}$$

where $H = [M_{AC} - L_C, M_{BC} - L_C]$.

$$\begin{bmatrix} L_A - M_{AC} & M_{AB} - M_{AC} \\ M_{AB} - M_{BC} & L_B - M_{BC} \end{bmatrix}^{-1} := \begin{bmatrix} H_{11} & H_{12} \\ H_{21} & H_{22} \end{bmatrix}.$$

Then, the state space model in continuous time domain can be simplified as

$$\dot{x}(t) = A_c x(t) + B_c u(t), \tag{5}$$

$$y(t) = C_c x(t), (6)$$

where

$$x = \begin{bmatrix} \psi_A(t) \\ \psi_B(t) \end{bmatrix}; y = \begin{bmatrix} i_A(t) \\ i_B(t) \end{bmatrix}; u = \begin{bmatrix} d_A(t) \\ d_B(t) \\ d_C(t) \end{bmatrix};$$

$$C_c = \begin{bmatrix} G_{11} + G_{13}H_{11} & G_{12} + G_{13}H_{12} \\ G_{21} + G_{23}H_{11} & G_{22} + G_{23}H_{12} \end{bmatrix};$$

$$B_c = \begin{bmatrix} 2/3 & -1/3 & -1/3 \\ -1/3 & 2/3 & -1/3 \end{bmatrix} V_{dc}; \quad A_c = -R_sC_c;$$

and V_{dc} is the DC bus voltage

III. MODEL PREDICTIVE CURRENT CONTROL FOR THE MCSRM

For digital implement of MPC approach, the continuoustime state-space description (5) and (6) of the plant is reformulated in discrete time domain with the standard form

$$x(k+1) = A(k)x(k) + B(k)u(k); (7)$$

$$y_c(k) = C_c(k)x(k); (8)$$

where x(k), u(k), $y_c(k)$ are the two phase flux linkage, duty ratio and phase current at time instant k; $A=e^{A_cT_s}$; $B=\int_0^{T_s}e^{A_c\tau}d\tau B_c$; T_s is the sampling period. Considering the motor control system is fast varying, the coefficient matrices in discrete time domain can be approximated by $A\approx 1+A_cT_s$; $B\approx T_sB_c$.

Before receding the prediction horizon, some modifications are made to the discrete dynamic model. Given that the system may have nonzero-mean input, a generalized incremental model for (7) and (8) is given to improve the minimization accuracy by

$$\triangle x(k+1) = A(k) \triangle x(k) + B(k) \triangle u(k) \tag{9}$$

$$\Delta y_c(k) = C_c(k) \Delta x(k); \tag{10}$$

where
$$\triangle x(k) = x(k) - x(k-1)$$
, $\triangle y_c(k) = y_c(k) - y_c(k-1)$, $\triangle u(k) = u(k) - u(k-1)$.

Based on the differential equation (9) and provided with a predictive horizon of p and a control horizon of m ($m \le p$), the system output $y_c(k+i\mid k)$ at time instant k+i can be derived after p-step iterations can be derived. It should be noted that coefficient matrices $A(k+i\mid k), B(k+i\mid k),$ and $C(k+i\mid k)$ are associated with the estimated inductances $L(k+i\mid k)$ and $M(k+i\mid k),$ that is, within the prediction horizon the inductances are updated.

The target of the model predictive current controller for the MCSRM is to keep the current response precisely tracking the reference current while achieving lower torque ripples. Accordingly, the cost function is set as

$$J = \sum_{i=1}^{p} \|\Gamma_{y,i}(y_c(k+i \mid k) - r(k+i))\|^2 + \sum_{i=1}^{m} \|\Gamma_{u,i} \triangle u(k+i-1))\|^2,$$
(11)

where $\Gamma_{y,i}=diag(\Gamma_{y1,i},\Gamma_{y2,i})$ is weight factor matrix for the two phase current tracking errors at predicted time instant $i;\;\Gamma_{u,i}=diag(\Gamma_{u1,i},\Gamma_{u2,i},\Gamma_{u3,i})$ is the weight factor matrix for the control input at predicted time instant $i;\;r(k+i)$ is the current reference sequence. In this paper, the current reference are the two phase sinusoidal waves. Thus, r(k+i) can be presented as $r_{1ref}(i+k)=14.5\sin(4(\theta_k-\delta+iT_sw_k)/180*\pi)$ and $r_{2ref}(i+k)=14.5\sin(4(\theta_k-\delta+30+iT_sw_k)/180*\pi)$, in which θ_k and w_k are the mechanical position and speed of the rotor at time instant $k;\;\delta$ is the leading angle.

So far, the optimal problem is formulated as finding the best three-phase duty ratio by minimizing the cost function (11). The control input of the model belongs to the range [-1,1]. Hence, the optimization problem in this paper is a constrained finite-control-set MPC problem. Therefore, the optimal control input $\triangle U^*(k)$ can be obtained by solving the cost function (12) subject to the discrete-time model (9) and (10) with respect to the input constraint which belongs to [-1,1], i.e., $u_{min}=-1, u_{max}=1$:

$$\min_{\triangle U(k)} J(x(k), \triangle U(k), m, p) \tag{12}$$

subject to $1 \ge U(k) \ge -1$.

Eventually, the first component of $\triangle U^*(k)$, i.e., $\triangle u^*(k)$, will be used to calculate the control input u(k) and be applied to the VSC.

$$\Delta u^*(k) = \begin{bmatrix} I_{3\times 3} & 0 & \cdots & 0 \end{bmatrix} \Delta U^*(k) \tag{13}$$

$$u(k) = u(k-1) + \triangle u^*(k) \tag{14}$$

IV. SIMULATION

In this section, the performance of the proposed model predicted current controller is first presented under different prediction horizon sizes and different control frequencies. The effectiveness of the controller is compared to hystersis current controller in terms of root mean square error (RMSE) and root mean square (RMS) value of the current and averaged torque. The RMSE, RMS current and averaged torque are defined as

$$I_{RMSE} = \sqrt{\frac{1}{45} \int_0^{45} (i_{ref} - i_k)^2 d\theta}$$
 (15)

$$I_{RMS} = \sqrt{\frac{1}{45} \int_0^{45} i_k^2 d\theta}$$
 (16)

$$T_{ave} = \sqrt{\frac{1}{45} \int_0^{45} T_k \mathrm{d}\theta} \tag{17}$$

The current references are the three phase sinusoidal waveform given by

$$\begin{cases} i_{ref_A} = I_m \sin[0.5N_p(\omega t - \delta)] \\ i_{ref_B} = I_m \sin[0.5N_p(\omega t - 30^\circ - \delta)] \\ i_{ref_C} = I_m \sin[0.5N_p(\omega t + 30^\circ - \delta)] \end{cases}$$
(18)

The nominal current of the MCSRM is 15A and the stator resistance for each phase is 0.3Ω . During the simulation, the PWM frequency for the MPC f_s is selected to be 10 kHz, 20 kHz, 30 kHz and 50 kHz for the purpose of comparison, which is the same as the control frequency.

A. Selection of switching frequency and prediction horizon

For a clear comparison, the prediction horizon and control horizon are of the same size, i.e., m=p. Though the weight factors in the cost function are important when solving the QP optimization problem, one can easily select appropriate weight factors to have the current response follow the current reference. In the following simulation results, the weight factors $\Gamma_{y,i}$ for limiting the current errors are selected to vary from 200 to 500; and weight factors $\Gamma_{u,i}$ for limiting the control input variations are selected to be 0.1 and keep unchanged. Thus, the weights in the following cases are not listed specifically.

Fig. 5 compares the simulation results at 500 rpm when the prediction horizon is 5 and control frequency is selected to be 10 kHz, 20 kHz, 30 kHz and 50 kHz. It is easy to understand that with higher switching frequency, the current tracking can be achieved with smaller variations, and thus the current response bears lower ripples and lower RMSE values. This is also demonstrated by Fig. 5. Besides, the torque response improves significantly as the switching frequency increases. This is directly resulted from good current response. For this reason, in order to achieve better current or torque performance regardless the power converter cost, increasing the switching frequency is a good method.

Fig. 6 is trying to find out the relation between the prediction horizon and performance quality at fixed switching frequency $f_s=20\,$ kHz. As can be seen from Fig. 6, none of the four cases stands out from the rest with significantly low current ripples. The simulation results show that the current ripples are slightly lower when $N_p=5$. This is because the tracking error would accumulate when the model doesn't fully match with the real plant. In this case, longer prediction horizon cannot gurantee the tracking accuracy. Likewise, too short prediction horizon is not able to sufficiently foresee the future states, and thus would fail in tracking as well. Additionally, longer prediction horizon leads to longer computation time and more requirements on the digital processor. Therefore, the prediction horizon should be carefully selected before implementing in the hardware.

The overall simulation evaluation at 1000 rpm are presented in Fig. 7. There is no doubt that with the highest switching frequency of 50 kHz, the current response has the lowest RMSE and the average torque curve is the steadiest whatever the prediction horizon is. However, for the most industrial application, 50-kHz switching frequency renders higher cost compared to the commonly adopted 10k-20kHz frequency. The trade-off between higher tracking accuracy and lower computation cost can be achieved when the tracking error falls in the tolerant range while the switching frequency and prediction horizon are appropriately selected. For example, in this simulation, $N_p=5$ and $f_s=20 \rm kHz$ can be a solution to maintain comparable performance.

B. Simulation comparison with hysteresis current control

Though Section A already demonstrates the current tracking ability of the finite control set MPC, it would be more

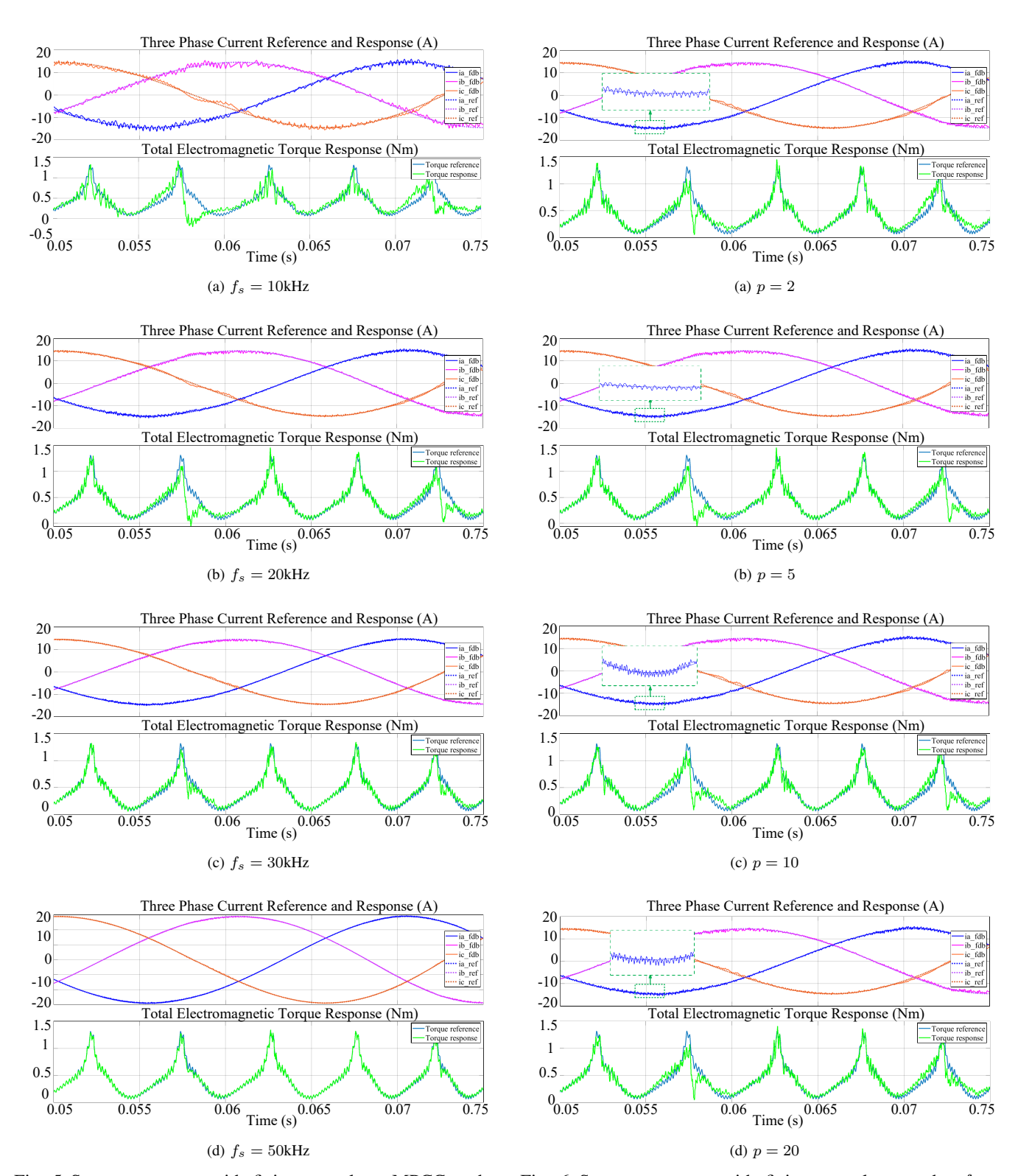
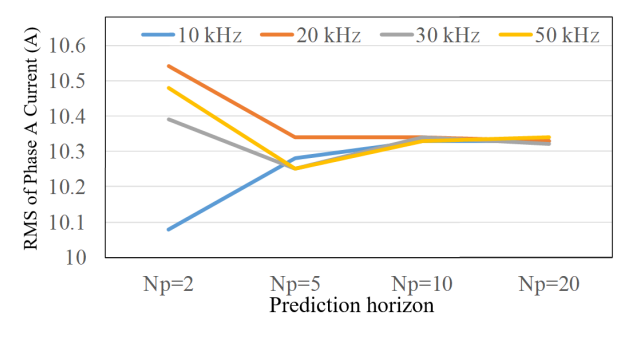
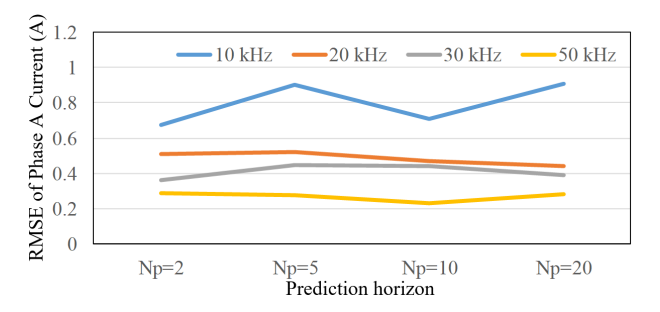


Fig. 5 System response with finite control set MPCC under p = 5.

Fig. 6 System response with finite control set under $f_s = 20 \text{kHz}$.



(a) RMS value of Phase A current



(b) RMSE value of Phase A current

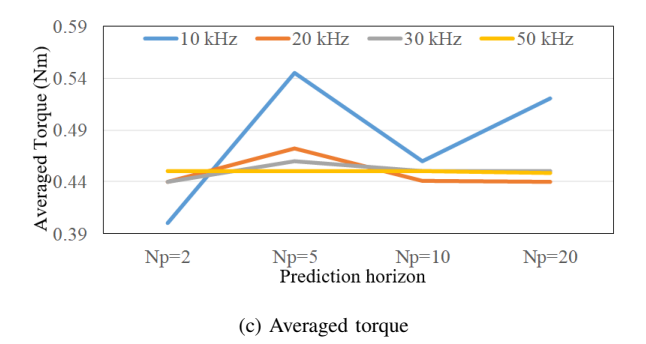


Fig. 7 System response evaluation under MPCC at 1000 rpm.

reasonable to compare it with a commonly applied controller for the machine. Both the finite control set MPC and hysteresis current control are good options in terms of fast dynamics and robustness.

Fig. 8 shows the current response with hysteresis current controller at 500 rpm when switching frequencies is limited to be no higher than 20 kHz by regulating the sampling rate and hysteresis band. Compared with Fig. 5, it is noticeable that both methods are capable of current tracking for the MCSRM while current response with MPCC has lower RMSE and a fixed switching frequency due to PWM technique. Hence, MPCC method shows great potential for further application on MCSRMs. Since this paper is the first trial of applying finite control set MPC to MCSRMs, more improvements such as reducing the computation burden and more accurately estimating the model can be explored.

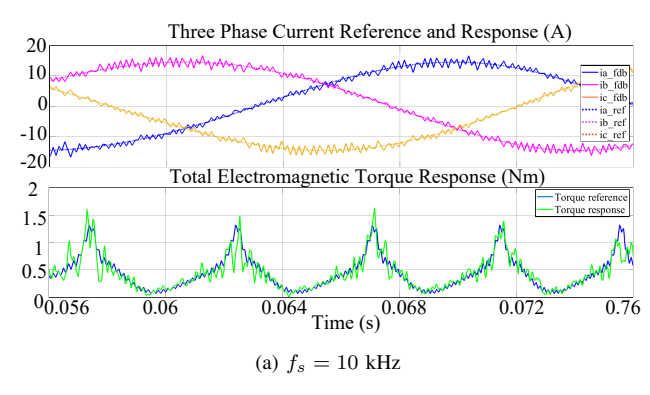


Fig. 8 System response with hysteresis control at 500rpm.

V. CONCLUSION AND FUTURE WORK

In this paper, a model predictive current control method is firstly proposed for the short-pitched MCSRMs using VSC to realize accurate current control. A two-order flux-based prediction model for the MCSRM combined with the VSC is derived with discrete state-space equations. Based on the prediction model, the optimal problem is formed aiming at minimizing the current error and duty cycle variation with the constraint on the duty ratio. By solving the constrained optimal control problem, the control input for the drive system is derived. Through simulation, the selection of switching frequency and prediction horizon has been discussed, and the current tracking ability for the MPCC is demonstrated. Compared to hysteresis current control, the current response with MPCC bears lower current ripples and a fixed switching frequency. The future work on this topic can be explorations on reducing the computation burden while maintaining excellent current tracking performance.

ACKNOWLEDGMENT

This work is partially supported by NSF-ECCS-1946057 and NSF-ECCS-1851875.

REFERENCES

- F. Peng, J. Ye, and A. Emadi, "A digital PWM current controller for switched reluctance motor drives," *IEEE Transactions on Power Electronics*, vol. 31, no. 10, pp. 7087–7098, 2016.
- [2] F. Yi and W. Cai, "Modeling, control, and seamless transition of the bidirectional battery-driven switched reluctance motor/generator drive based on integrated multiport power converter for electric vehicle applications," *IEEE Transactions on Power Electronics*, vol. 31, no. 10, pp. 7099–7111, 2016.
- [3] C. Gong and T. Habetler, "A novel rotor design for ultra-high speed switched reluctance machines over 1 million rpm," in 2017 IEEE International Electric Machines and Drives Conference (IEMDC). IEEE, 2017, pp. 1–6.
- [4] G. Li, J. Ojeda, E. Hoang, M. Lécrivain, and M. Gabsi, "Comparative studies between classical and mutually coupled switched reluctance motors using thermal-electromagnetic analysis for driving cycles," *IEEE Transactions on magnetics*, vol. 47, no. 4, pp. 839–847, 2011.
- [5] W. Ding, Y. Hu, and L. Wu, "Investigation and experimental test of fault-tolerant operation of a mutually coupled dual three-phase srm drive under faulty conditions," *IEEE Transactions on Power Electronics*, vol. 30, no. 12, pp. 6857–6872, 2015.

- [6] G. Li, X. Ojeda, S. Hlioui, E. Hoang, M. Gabsi, and C. Balpe, "Comparative study of switched reluctance motors performances for two current distributions and excitation modes," in 2009 35th Annual Conference of IEEE Industrial Electronics. IEEE, 2009, pp. 4047– 4052.
- [7] R. Pupadubsin, N. Chayopitak, S. Karukanan, P. Champa, P. Somsiri, and K. Tungpimolrut, "Comparison of winding arrangements of three phase switched reluctance motor under unipolar operation," in 2012 15th International Conference on Electrical Machines and Systems (ICEMS). IEEE, 2012, pp. 1–4.
- IEEE, 2012, pp. 1–4.
 [8] A. C. Clothier, "Switched reluctance motor drives with fully pitched windings," Ph.D. dissertation, Newcastle University, 2001.
- [9] X. Liang, G. Li, J. Ojeda, M. Gabsi, and Z. Ren, "Comparative study of classical and mutually coupled switched reluctance motors using multiphysics finite-element modeling," *IEEE Transactions on Industrial Electronics*, vol. 61, no. 9, pp. 5066–5074, 2013.
- [10] K. Hu, J. Ye, J. M. Velni, L. Guo, and B. Yang, "A fixed-switching-frequency sliding mode current controller for mutually coupled switched reluctance machines using asymmetric bridge converter," in 2019 IEEE Transportation Electrification Conference and Expo (ITEC). IEEE, 2019, pp. 1–6.
- [11] J. Ye, P. Malysz, and A. Emadi, "A fixed-switching-frequency integral sliding mode current controller for switched reluctance motor drives," *IEEE Journal of Emerging and Selected Topics in Power Electronics*, vol. 3, no. 2, pp. 381–394, 2015.
- [12] K. M. Rahman, B. Fahimi, G. Suresh, A. V. Rajarathnam, and M. Ehsani, "Advantages of switched reluctance motor applications to ev and hev: Design and control issues," *IEEE transactions on industry applications*, vol. 36, no. 1, pp. 111–121, 2000.
- [13] S. Kouro, P. Cortés, R. Vargas, U. Ammann, and J. Rodríguez, "Model

- predictive control—a simple and powerful method to control power converters," *IEEE Transactions on industrial electronics*, vol. 56, no. 6, pp. 1826–1838, 2008.
- [14] X. Li and P. Shamsi, "Model predictive current control of switched reluctance motors with inductance auto-calibration," *IEEE Transactions* on *Industrial Electronics*, vol. 63, no. 6, pp. 3934–3941, 2015.
- [15] H. Peyrl, G. Papafotiou, and M. Morari, "Model predictive torque control of a switched reluctance motor," in 2009 IEEE International Conference on Industrial Technology. IEEE, 2009, pp. 1–6.
- [16] X. Li and P. Shamsi, "Inductance surface learning for model predictive current control of switched reluctance motors," *IEEE Transactions on Transportation Electrification*, vol. 1, no. 3, pp. 287–297, 2015.
- [17] R. Mikail, I. Husain, Y. Sozer, M. S. Islam, and T. Sebastian, "A fixed switching frequency predictive current control method for switched reluctance machines," *IEEE Transactions on Industry Applications*, vol. 50, no. 6, pp. 3717–3726, 2014.
- [18] S. Mehta, M. A. Kabir, and I. Husain, "Extended speed current profiling algorithm for low torque ripple srm using model predictive control," in 2018 IEEE Energy Conversion Congress and Exposition (ECCE). IEEE, 2018, pp. 4558–4563.
- [19] M. F. Q. Maidana, W. A. da Silva, W. B. Correia, B. C. Torrico, and F. G. Nogueira, "Comparative study of pi-aw and mpc-t controllers, with feedback noise applied for speed control to a switched reluctance motor (srm)," in 2017 Brazilian Power Electronics Conference (COBEP). IEEE, 2017, pp. 1–6.
- [20] J. Ye and F. Hensley, "Torque ripple and copper loss minimization for a family of mutually coupled switched reluctance machines," in 2017 IEEE Applied Power Electronics Conference and Exposition (APEC). IEEE, 2017, pp. 546–551.